



Scopus® doi

# Journal of Vibration Engineering

ISSN:1004-4523

Registered



SCOPUS



GOOGLE SCHOLAR



DIGITAL OBJECT  
IDENTIFIER (DOI)



IMPACT FACTOR 6.1



Our Website  
[www.jove.science](http://www.jove.science)

## ABSTRACT

In light of the fact that the majority of power electronics utilised in photovoltaic (PV) inverters at commercial and industrial sites behave as non-linear loads from the grid side, these high-power the power quality of the network is anticipated to be significantly impacted by demand installations. This study provides a complete framework to help with their integration into the distribution grid. Quasi-Z Source T-Type PV inverter control technique that uses the spare inverter power capacity to execute active and reactive power regulation, harmonic and imbalance correction, and imbalance compensation. Contrary to other methods, the one put forth here functions properly under distorted and imbalanced grid voltages. When assessing how the suggested technique works with three-phase PV inverters, the electrical network architecture inside a commercial and industrial site is taken into account.

Due to the power topology's capacity to raise the voltage, it is not necessary to employ the standard step-up transformer and/or supplementary DC-DC converter found in PV inverter systems. The effectiveness of the suggested technique is illustrated using a 50 kW converter model with a disrupted grid environment and fluctuating load conditions.

## INDEX TERMS

Grid-connected PV inverters, commercial and industrial Nano grids, and reactive power compensation, compensation for harmonics and imbalance, and quasi-impedance-source T-type inverters.

## I. INTRODUCTION

The aggregation of renewable energy sources (RES), particularly those that are sporadic, non-dispatchable, or unpredictable, creates significant difficulties for electricity grid design and operation. The function of Nano grids in this situation becomes crucial. Nano grids, in essence, are just tiny micro grids that typically serve one or a few buildings or facilities. Commercial and Industrial Nano grids (CINs), which include factories or office buildings, have attracted more attention in recent years. DC voltage is produced by the majority of RES, including fuel cells and photovoltaic (PV) modules. Therefore, power produced by RES should generally be in condition. In this instance, grid-interactive PV inverter explicitly performs this procedure, which is typically handled by power electronics systems (PVI). The traditional voltage source inverter (VSI), one of the topologies most frequently utilised in these converters, has several limitations. The DC input voltage must be greater than the peak grid voltage. The DC voltage levels generated in practical applications, such PV systems, are typically modest and subject to large variations depending on the operating circumstances. In order to raise the DC voltage, a second DC-DC converter is needed. Utilizing a step-up transformer is an additional alternative. Alternately, the use of an impedance source (Z-source) inverter can do away with the need for both an extra DC-DC converter and/or a step-up transformer. The Z-source network, which is made up of two capacitors and two inductors, connects the DC bus terminals to the inverter input. This approach allows for the employment of the so-called Shoot-Through (ST) states, which are utilised to generate voltage boost, in addition to the well-known switching combinations used in VSIs, which produce the so-called Non-Shoot-Through (NST) states. A topology known as a quasi-impedance source inverter (quasi-Z-source) was introduced as a further advancement. However, several studies have found advantages to using three-level inverters in PV systems. By switching only half the DC link voltage, this architecture exhibits reduced switching losses and lower harmonic contents in the output voltage than the two-level inversion one. A well-known member of this family is the neutral-point-clamped (NPC) inverter; a more recent member is the T-type inverter, which offers significant gain over NPC by lowering switching losses at lower switching frequencies. An intriguing idea is the combination of a quasi-Z network and a three level inverter. More specifically, it has been thought about to combine a quasi-Z network with a three level T-type inverter. In any case, the majority of converters exhibit non-linear behaviour and demand distorted and unbalanced currents from the AC grid. As a result, a complete installation's currents will be disturbed and out of balance when observed from the AC side. Grid voltages will be distorted as a result of these current demands and those made by nearby facilities linked to the same distribution feeder. The majority of PVI control solutions in the technical literature attempt to avoid adding further distortion while adhering to the suggested limits. Nevertheless, when the grid voltages are distorted and/or imbalanced, such solutions fail to function properly. It is important to mention at this point that electronic power converters have the capacity to operate actively and, as a result, can perform auxiliary tasks for the electrical system, such as frequency and voltage regulation and power quality enhancement. There are a lot of published papers on three-phase grid interactive inverters, but not many on grid interactive inverters based on Z-source or quasi-Z-source converters. Most research on this topology is primarily concerned with modulation methods and capacitor voltage balance difficulties. While many studies use Z-source and 2-level VSI, references deal with Z-Source-T-type and quasi-Z-Source T-type topologies, respectively, with grid control but do not implement corrective measures. A grid control approach with compensating action was recently put into practise by the authors, although it has not been demonstrated that it performs well when the grid voltage is distorted.

As a result of the foregoing, it is still necessary to enhance and expand the functions that can be provided by electronic converters, which can be done by researching various topologies along with better control strategies. This will help to facilitate the increasing integration of RES into the network. These are this paper's primary contributions:

1. The incorporation of PV inverters into a commercial and industrial Nano grid that is based on a three-phase Quasi-Z-Source Three-Level T-Type topology. The control strategy I integrates several functions that have been partially implemented on this particular power topology, such as active and reactive power control, harmonics and imbalance mitigation, (ii) suggests a cooperative operation between inverters inside the CIN, and (iii) in any case, performs well under distorted and unbalanced grid voltage, extending the successes reported.
2. The control strategy is simple and may be used to coordinate or operate independently to achieve harmonic and imbalance mitigation, reactive power compensation, and optimal PV power injection into the grid. Furthermore, the DC link capacitors found in PV's AC/DC converters allow them to be employed as active filters even when there isn't any sunlight. No matter what process the power electronics equipment is used in, the concept aims to maximise its benefits. The remaining parts of the essay are arranged as follows. Following the configuration of a PV-based CIN, a detailed explanation of the inverter structure, control scheme, modulation method, and current controller is provided.

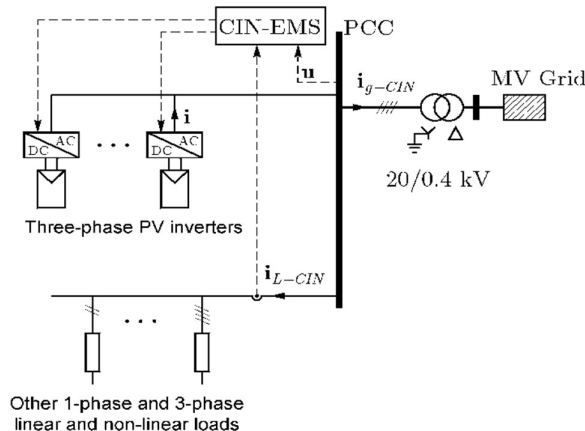
## II. POWER STRUCTURE AND CONTROL SYSTEM

Figure 1 depicts the structure of a typical CIN case. Using an MV/LV transformer, a total power of between 1000 and 1500 kW is connected to the Medium Voltage (MV) distribution network. The Low Voltage (LV) network contains four wires, three phases, and 230/400V, with the neutral grounded at the transformer neutral in accordance with the TT grounding scheme, and it can supply both single-phase and three-phase loads.

### A. TOPOLOGY

The proposed topology for PVI is depicted in Figure 2. This T-type inverter features three levels, three phases, and a quasi-Z source. The quasi-Z network, the T-type three-level inverter, the output filter, and the DC voltage source—which represents a renewable energy source—are all shown in the figure. While the currents from each individual PVI are  $I_A, I_B, I_C$ , the voltage and current from the PV panels are  $U_{PV}$  and  $I_{PV}$ , respectively. Figure 2 also depicts the assigned portion of the unbalanced and non-linear load on the CIN (which will be further specified). The CIN injects  $I_{GA}, I_{GB}, I_{GC}$  total currents into the grid, whereas this load requires  $I_{LA}, I_{LB}, I_{LC}$  total currents.

The terminals P, 0, or N are connected to the outputs (a', b', and c') of the inverter using various switching combinations. The result is a waveform with three voltage values ( $U_{PN}/2, 0$  and  $U_{PN}/2$ ). These NST states represent the corresponding switching combinations. The output is zero-voltage when the upper ( $S_1$ ) and lower ( $S_2$ ) switches of each phase are closed, joining the P and N points. The one being discussed is the aforementioned ST condition, which is not allowed in a conventional VSI (without the Z-source network), because it causes a short circuit in the DC source. The duty cycle of the ST state can be altered to raise the DC bus voltage.



**Fig.1.** Photovoltaic (PV) based CIN architecture.

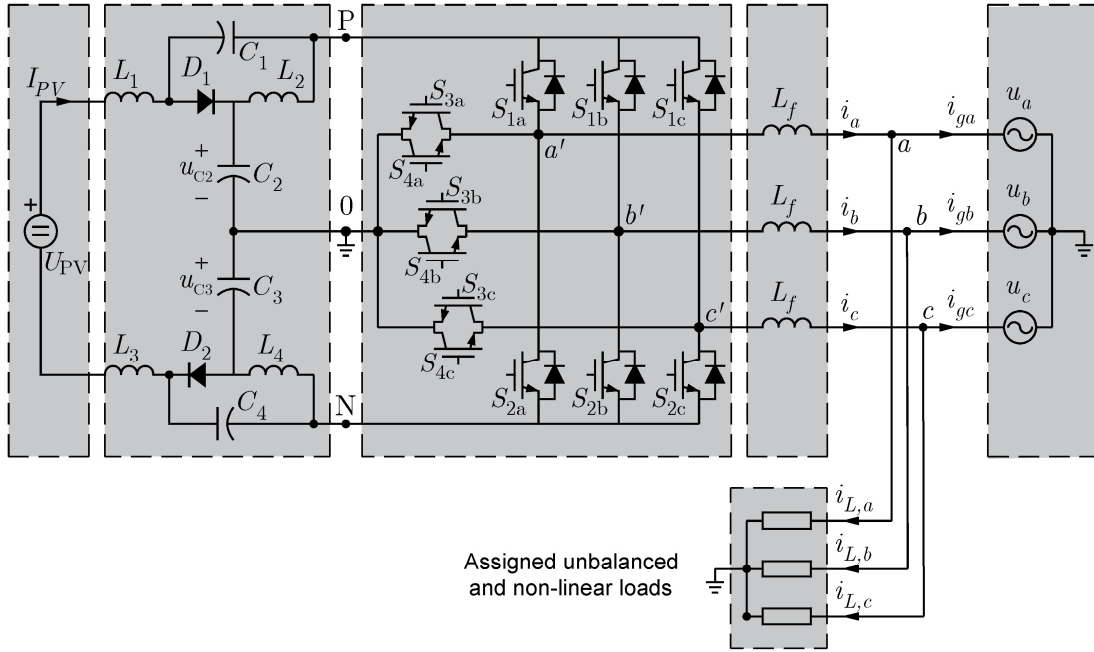


**Fig.2.** Three-phase topology for one PV inverter (PVI) and the assigned fraction of the facility's unbalanced and non-linear loads.

The switching period  $T = T_N + T_0$  is used to define the durations of the NST and ST states, and the related duty ratios are  $D_N = T_N/T$  and  $D_0 = T_0/T$ . The voltages across the passive components are  $u_{L1} = u_{L3}$ ,  $u_{L2} = u_{L4}$  and  $u_{C1} = u_{C4}$ ,  $u_{C2} = u_{C3}$  assuming that the quasi-Z-source network is symmetric (i.e.,  $L_1 = L_3$ ,  $L_2 = L_4$  and  $C_1 = C_4$ ,  $C_2 = C_3$ ). The converter is also supposed to run in continuous conduction mode. Taking into account that, in steady state, the average voltage value at the inductor terminals during each switching period is zero. The boost factor  $B$  is defined from:

$$B = \frac{\hat{U}_{PN}}{U_{PV}} = \frac{1}{1 - 2D_0}$$

where  $\hat{U}_{PN}$  is the peak DC-link voltage, available during NST states.

The amplitude of the fundamental component of the output phase-to-neutral voltage is given by:

$$\hat{U}_{an,1} = m \frac{\hat{U}_{PN}}{2} = m \frac{1}{1 - 2D_0} \frac{U_{PV}}{2}$$

where  $m$  is the modulation index.

## B. PROPOSED CONTROL STRATEGY

In order to achieve the active power and reactive power setpoint offered by the CIN-EMS, the reference current for each PVI of a CIN,  $I^* = (I_a^* I_b^* I_c^*)^T$  (see Figures 1 and 2) is calculated using the control strategy. It is also possible to achieve harmonic and imbalance compensation at the PCC if the PVI rated power is not exceeded. In order to provide balanced and sinusoidal currents with displacement power factor (DPF) in accordance with CIN-EMS criteria, each PVI works together to improve the performance of the LV network. With a minimum amount of error between the measured and reference currents, the tracking technique obtains the switching signals for the PVI.

The three elements that make up the PVI reference current vector are reactive power  $I_P^* = (I_{Pa}^* I_{Pb}^* I_{Pc}^*)^T$ , reactive power  $I_Q^* = (I_{QA}^* I_{QB}^* I_{QC}^*)^T$ , and harmonic and imbalance load current  $I_{HI}^* = (I_{HIA}^* I_{HIB}^* I_{HIC}^*)^T$ . These terms are explained in more detail in the following sections.

The block diagram of the PVI control system is shown in Figure 3, where  $P^*$  and  $Q^*$  are set by the CIN-EMS and  $I_L$  is determined at the PCC.

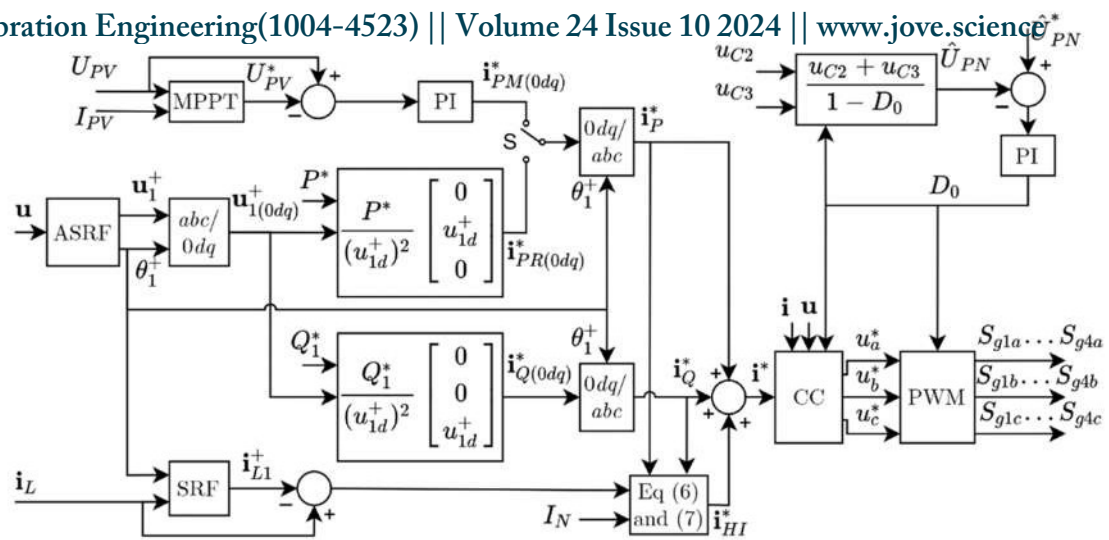


**Fig.3.**Block diagram of the PVI controls system.

### C. ACTIVEPOWERCONTROL(PMODE)

In order to make the current injected into the grid proportional to the positive-sequence fundamental grid voltage, a modified version of the Perfect Harmonic Cancellation (PHC) control approach is suggested. It makes sure the PVI runs on a unity DPF that delivers sinusoidal and balanced current. Maximum Power Point Tracking mode (MPPT mode) and Reference Power Point Tracking are the two operational modes that are taken into consideration for this Pmode (RPPT mode). An MPPT algorithm, such as the traditional Perturb and Observe, will be used to determine the reference PVI current in the  $0dq$  reference frame when the MPPT mode is active (chosen by the switch S), based on local voltage and current measurements from the PV panels connected to the specific PVI.

However, in the RPPT mode, the CIN-EMS assigns a three-phase active power set point  $P_{to}$  to every individual PVI based on a variety of parameters that depend on commercial or economic considerations, which are outside the purview of this article. To provide some examples in this area might be fascinating, though. Therefore, the RPPT mode could be used if the inverter briefly stops producing power and makes use of all of its capabilities to function as a static synchronous compensator (STATCOM), as suggested in. Additionally, if a PVI is connected to an energy storage system, such as one based on batteries, the system may inject a reference constant active power into the grid periodically.

If the batteries are fully charged and the solar irradiation is too great in this situation, it may be necessary to limit the power from the PV panels. Therefore the PV current in the 0dq reference frame is derived in this study from the previously mentioned reference power set point  $P^*$  by the following current vector when the RPPT mode is engaged (chosen by the switch S in Figure 3).

$$\mathbf{i}_{PR(0dq)}^* = \frac{P^*}{(u_{1,d}^+)^2} \begin{bmatrix} 0 \\ u_{1,d}^+ \\ 0 \end{bmatrix},$$

A positive-sequence fundamental vector,  $U_1^+$ , and its phase angle are extracted from the grid voltage  $U$  via an Auto-Adjustable Synchronous Reference Frame (ASRF) phase-locked-loop. After that, the Park transformation is applied by the block  $abc/0dq$ .

#### D. REACTIVEPOWERCONTROL(Q-MODE)

Reactive power management or PCC voltage support may be offered by the CIN for commercially viable reasons based on tariff incentives. Thus, the CIN-EM transmits to each unique PVI a fundamental three-phase reactive power setpoint  $Q_1^*$ . The fundamental reactive power flow from the grid to the PVI ( $Q_1^* < 0$ ) and the fundamental reactive power flow from the PVI to the grid ( $Q_1^* > 0$ ) are the two operational modes that are taken into consideration.

A proposed control approach that derives from the PHC strategy tries to have the PVI deliver balanced current that is sinusoidal and lags 90 degrees after the grid voltage's positive-sequence fundamental component. As a result, the reference PVI current in Q mode is determined as follows in the 0dq reference frame:

$$\mathbf{i}_{Q(odq)}^* = \frac{Q_1^*}{(u_{1,d}^+)^2} \begin{bmatrix} 0 \\ 0 \\ u_{1,d}^+ \end{bmatrix}$$

Likewise, the reference current vector in the abc frame  $I_Q^*$  is obtained by means of the inverse transformation 0dq/abc.

This mode seeks to balance the unbalanced and harmonic currents required by the CIN loads such that the PVI acts as an Active Power Filter (APF). This results in improved power quality and imbalance ratios in the CIN due to the involvement of all PVIs. The CIN-EMS computes portions ( $i_L$ ) for each PVI based on the total load current at the PCC ( $i_{L-CIN}$ ), which is measured and divided by the CIN-EMS. While this is going on, the phrases below can be used to dissect the load current assigned to a PVI. A Total Harmonic and Imbalance Compensation (THIC) control strategy is proposed aiming that the PVI current is equal and opposite to the harmonic and fundamental unbalanced components of  $i_L$ , that is:

$$i_{HI}^* = -(i_L - i_{L1}^+)$$

By utilising the positive-sequence fundamental phase angles supplied by the ASRF block, the Synchronous Reference Frame (SRF) block is responsible for extracting  $i_{L1}^+$  from the allocated load current vector  $i_L$ . In order to prevent the PVI from exceeding its nominal current  $i_N$ , the reference current in Equation (5) must be saturated. As a result, the reference current's Root Mean Square (RMS) value for the HI mode is determined to be

$$I_{HI,max} = \sqrt{I_N^2 - I_P^2 - I_Q^2}$$

where  $I_P$  and  $I_Q$  are the RMS values for  $I_P^*$  and  $I_Q^*$ , respectively. Finally, the reference PVI current is obtained from the equations below.

$$i_{HI}^* = -(i_L - i_{L1}^+) \quad \text{if } I_{HI} \leq I_{HI,max}$$

$$i_{HI}^* = -(i_L - i_{L1}^+) \frac{I_{HI,max}}{I_{HI}} \quad \text{if } I_{HI} > I_{HI,max}$$

where  $I_{HI}$  is the highest RMS value of the components of  $i_{HI}^*$ . The part that performs the THIC strategy appears at the bottom of Figure 3.

## F. CURRENT CONTROLLER AND MODULATION METHOD

A current controller (block designated CC in Figure 3) will be utilised after the current references have been defined to make sure that the inverter output currents follow those references. To control the present error ( $\Delta i$ ) a straight forward proportional controller is chosen. This proportional controller is actually set to change the desired maximum current ripple, which is expressed as a percentage of the nominal current. By taking into account the constraint  $U_Y^* < 1 - D_0$ , where  $y$  stands for the phase  $a, b, \text{ or } c$ , a saturation block restricts the maximum and minimum values of the control signals. In the part that follow, a precise and quick transient response of this controller with no steady error will be demonstrated. This is the implementation block diagram is represented in figure 4.

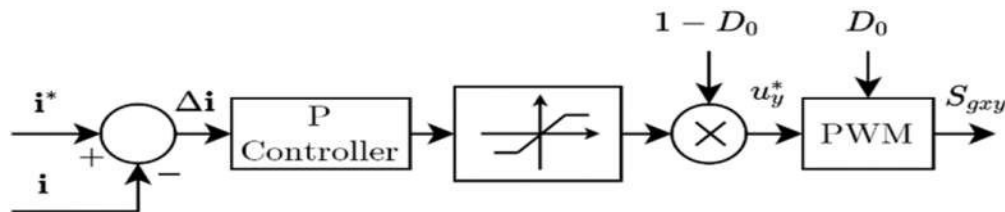


**Fig.4.** Block diagram of the current controller and modulator

The duty cycle to be used on each branch of the network is determined by each signal denoted as  $U_Y^*$  an inverter. As a switched duty cycle is reached because this control action is computed as a proportional value of the difference between the measured  $I$  and the instantaneous reference  $I^*$  (with a switched form), as shown in Figure 5. The different gate signals ( $S_{gxy}$ ), where  $x$  represents the switch (1,...,4) for the power converter, are then generated using a level-shifted pulse width modulation (LS- PWM) in phase disposition with constant boost control (CBC).



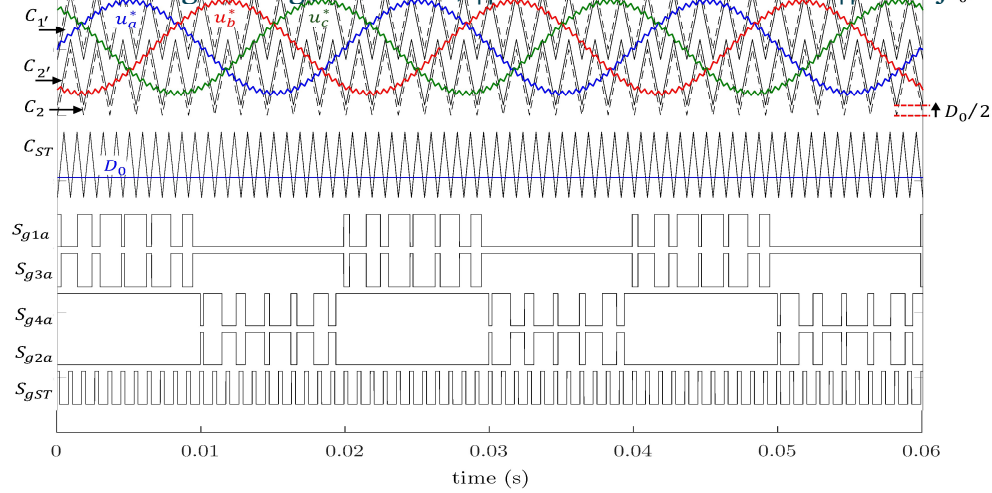


**Fig.5.** Switching signal generation with the level-shifted pulsewidth modulation (LS-PWM) in phased disposition with the constant boost control (CBC) scheme.

The layout of the LS-PWM in phase arrangement with CBC is shown in Figure 5. For better viewing, a frequency modulation index of 11 has been employed. To create the NST states and activate the various power switches, the three signals  $U_y^*$  and two carrier signals (upper [0, 1] and bottom [-1, 0]) are compared. The NST states for branch a, for instance, are shown in the same image. In reaction to the ST state generation indicated by  $D_0$ , another carrier with a double frequency is present. When the ST states are regenerated in this manner, they are uniform and have a constant width during the basic period. Finally, carriers  $C_1$  and  $C_2$  are shifted. The value of  $D_0/2$  to compensate the output average voltage which is affected due to ST states insertion.

## G. DC BUS VOLTAGE REGULATION

The peak voltage  $U_{PN}$  in Z-source inverters is the DC-link voltage that is present during NST states. By modifying  $D_0$  in accordance with the equation (1), the variable PV voltage  $U_{PV}$  value—which is brought about by changes in solar irradiance or reference power—can be controlled. The DC-link voltage is a pulsed voltage waveform, hence it must be kept in mind that it cannot be utilized as a feedback signal. So, a deceptive strategy is used. The voltages of capacitors  $C_1, C_2$ , and  $C_3$  are measured, and the following relation is used to compute the actual peak DC-link voltage:

$$u_{C2} + u_{C3} = (1 - D_0) \hat{U}_{PN}$$

The difference between the reference magnitude  $\hat{U}_{PN}^*$  and the estimated magnitude  $\hat{U}_{PN}$  is seen in Figure 3's top right corner. The ST duty-cycle  $D_0$  is then produced by processing the error signal by a Proportional Integral (PI) controller. The PWM stage's input consists of this duty cycle and the output of the current controller.

## III. SIMULATION RESULTS AND ANALYSIS

The current study is concentrated on PVI power range of 50-200 kW, which is suitable for commercial, industrial, and multi-megawatt PV systems. A PVI with the following rating, more particularly, is taken into account: 230/400V; 50Hz, 50kW. A 72.5 rated RMS current is the corresponding value. The key equipment specs are included in Table 1. According to the following equations were used to determine the source network's component parts:

$$C_{1,4} \geq \frac{2P_{out}(1 - 2D_0)}{U_{PV}^2 f_{sw} K_C} \quad (9)$$

$$C_{2,3} \geq \frac{2P_{out}(1 - 2D_0)D_0}{U_{PV}^2 f_{sw} K_C (1 - D_0)} \quad (10)$$

$$L_{1,2,3,4} \geq \frac{U_{PV}(1 - D_0)D_0}{2I_{PV} f_{sw} K_L (1 - 2D_0)} \quad (11)$$

Along with the previously mentioned variables, the following terms are used in these equations:  $f_{sw}$ ,  $K_L$ , is the assumed ripple in  $I_{PV}$ ,  $P_{out}$  is the rated output power, and  $K_C$ , is the maximum voltage ripple across the capacitors.

An output filter made up of the inductors  $L_f$  reduces the output voltage harmonic distortion at the switching frequency. The values of these inductors are derived using [36] from the equation below.

$$L_f \geq \frac{U_{INV}^2}{2\pi f_1 \cdot h_{SW} \cdot P_{out} \cdot THD_1} \quad (12)$$

where  $U_G$  is the RMS grid voltage (phase-to-neutral),  $F_1$  is the fundamental frequency,  $H_{SW}$  is the switching harmonic order,  $THD_1$  is the anticipated total harmonic distortion of the output current, and  $U_{INV}(H_{SW})$  is the desired harmonic distortion of the output voltage at the switching frequency.

Other than the PVI itself, an equivalent load representing of the linear and non-linear loads on the CIN is taken into account. This load's rated apparent power requirement ought to be roughly equal to the total installed PV power in the CIN. As a result, the CIN could run in off-grid mode. The CIN-EMS measures the CIN's load current ( $I_{L-CIN}$ ) at the PCC and gives each PVI a fraction ( $I_L$ ). Harmonic analysis and the accompanying correction procedures, according to commercial buildings and industrial plants, are necessary when a significant amount of non-linear loads (usually larger than 25% to 30% of the total load) is already present or is predicted to be added. Therefore, harmonic and imbalance correction over around 40% of the entire demand for the CIN is suggested in this work as a representative example. As a result, the load RMS current assigned to a particular PVI will be roughly 40% of the PVI's rated RMS current,  $I_L = 30$  A in this case.

**Table 1.** Main parameter values for the 3-phase PVI

PARAMETER	VALUE	UNIT
Inductors $L_1, L_4$	0.5	MH
Capacitors $C_1, C_4$	2.2	MF
$L_f$	0.75	MH
Voltage output filter	800-1100	V
$U_G$	230	V
K <sub>L</sub> and K <sub>C</sub> (output voltage)	0.05	P.U.
$U_{INV}(H_{SW})$	0.05	P.U.
THD <sub>1</sub>	0.05	P.U.
Power output rating $P_{out}$	50	KW

The PSCAD simulation programme has been used to create a simulation model for a PVI under the aforementioned conditions. With a simulation time step of  $10^{-6}$  s, the switching frequency and sampling rate were both set to 10 kHz. It was intended for the four-wire LV network to be imbalanced and distorted. While the percentages for harmonics 5 and 7 are computed for having a Total Harmonic Distortion (THD) within the 8% limit, the individual distortion percentage for harmonic 3 is chosen at its maximum level. The zero-sequence component ( $U^0$ ) is added with the inverse sequence component ( $U^-$ ) set at its maximum value. Table 2 displays these numbers.

Table 2. Low Voltage (LV) network characteristics.					
Voltage Harmonic Distortion (%)			Voltage THD (%)	$U^-/U^+$ (%)	$U^0/U^+$ (%)
HD3	HD5	HD7			
5	4.5	4	7.83	2	2

$U^+, U^-, U^0$ : positive-, negative- and zero-sequence fundamental components.

Figures 6 to 10 show the outcomes of the simulation. With two distinct PV voltages starting at  $t=0$ , the simulation begins under two different solar irradiation circumstances.  $U^* = 1060$  V is chosen as the necessary DC link voltage. The ST control and the three control modes (P, Q, and HI) are returned on at  $t=0.2$  s. Considered are the cases listed below.

- Case A: PV voltage set to  $U_{PV} = 1060$  V. MPPT mode.  $P^* = 50$  kW;  $Q_1^* = 0$ ; CIN load without harmonics or imbalance; injecting active power close to rated power with no reactive power.
- Case B: RPPT mode with PV voltage set to  $U_{PV} = 850$  V. Active and reactive power injection:  $P^* = 45$  kW;  $Q_1^* = 21.7$  KVAR. CIN's load is unbalanced and harmonic-free.
- Case C: RPPT mode with PV voltage set to  $U_{PV} = 850$  V. Active and reactive power injection:  $P^* = 45$  kW;  $Q_1^* = 15$  KVAR. The maximum load for CIN with odd harmonic currents is the ninth order. Table 3 displays harmonic and imbalance content. According to standard calculations, the corresponding current's RMS value for this load is  $I_{LE} = 31.53$  A. The purpose of HI compensation is not activated.
- Case D: RPPT mode, PV voltage set to  $U_{PV} = 850$  V. injecting  $P^* = 45$  kW of both active and reactive electricity;  $Q_1^* = 15$  KVAR. Harmonic and unbalanced load characteristics of CIN as in instance C. The HI compensating feature is turned on.



- Case E: RPPPT mode, PV voltage set to  $U_{pv} = 850V$ , Active and reactive power injection  $P^* = 45kW$ ,  $Q^* = 21.7KVAR$ , respectively. Content of the CIN's load that is harmonic and unbalanced, as in examples C and D. The HI compensation feature is active.

In situations A (Figure 6) and B (Figure 7), the CIN load current is sinusoidal and balanced, hence the reference current for the HI control is zero. In example A, the CIN-EMS does not supply a reactive power setpoint; as a result, the MPPT algorithm just activates the P control with a reference value. By injecting a current into the grid in phase with the positive-sequence fundamental grid voltage, the PVI achieves a unity DPF. In scenario B, the CIN-EMS transmits active and reactive power setpoints to the PVI. The DC-link voltage is near to its reference value in both scenarios, as can be shown.

Table 3. Harmonic content of the Commercial and Industrial Nanogrids (CIN) current for cases C-E.

Individual Harmonic Distortion (% Respect to the Positive-Sequence Fundamental Component)				Total Harmonic Distortion THD (%)	$I^-/I^+$ (%)	$I^0/I^+$ (%)
HD3	HD5	HD7	HD9			
21.6	10.7	7.2	3.8	25.44	10	10

$I^+$ ,  $I^-$ ,  $I^0$ : positive-, negative- and zero-sequence fundamental components.

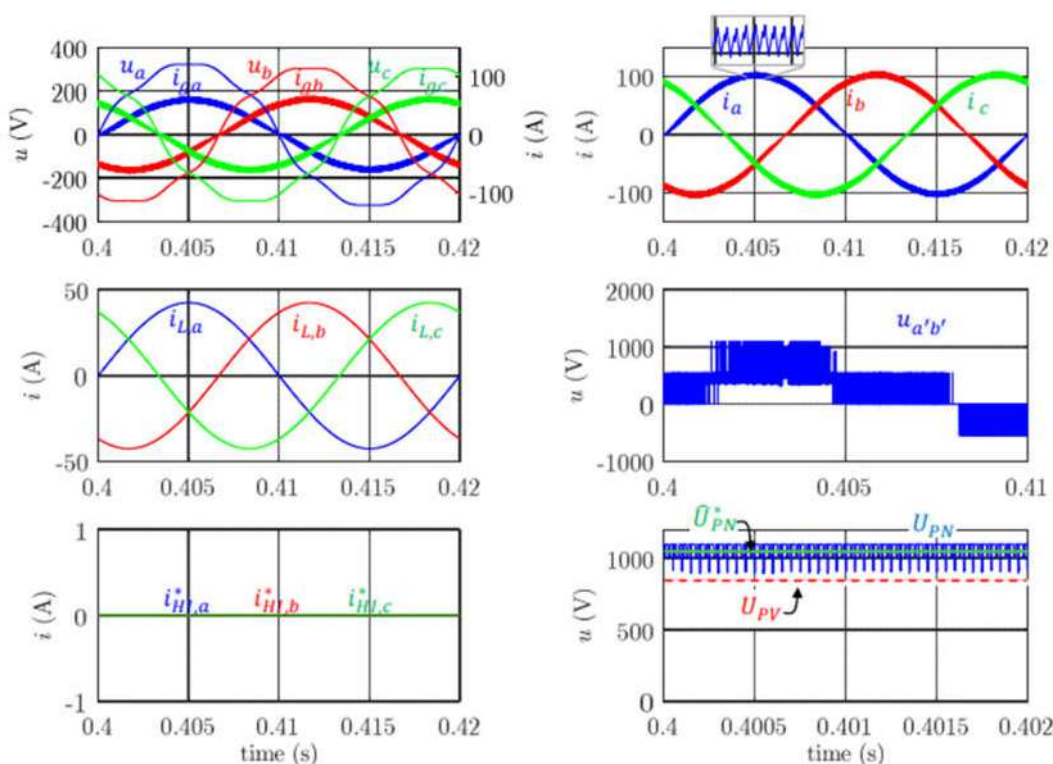
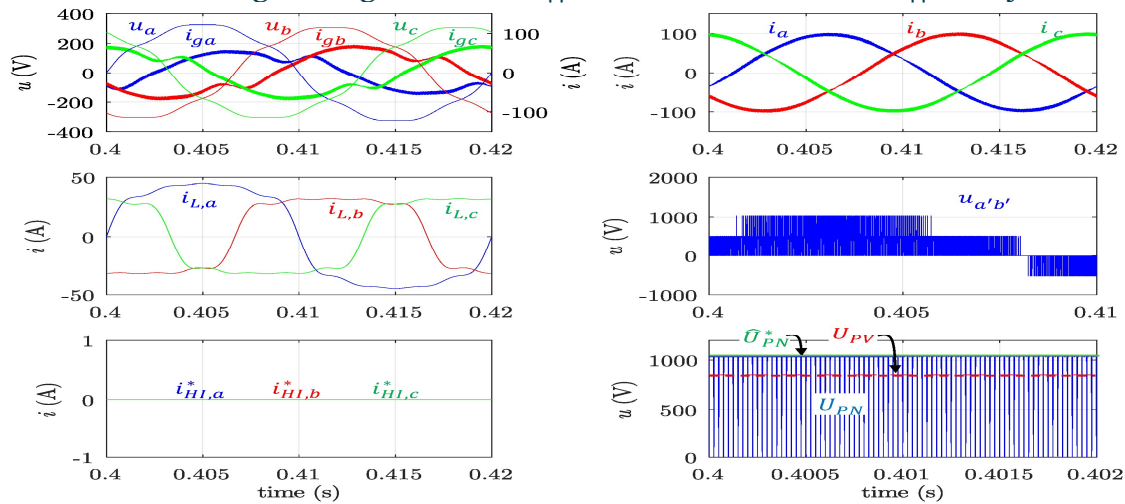


Figure 6. Simulation outcomes. CIN setpoints (delivered at  $t = 0.2s$ ) in Case A: CIN load with no harmonics or unbalance, and  $P^* = 50kW$ ;  $I_L = 30A$ . Left to right and top to bottom, respectively: gridded voltages ( $U_A, U_B, U_C$ ), grid currents ( $I_{GA}, I_{GB}, I_{GC}$ ), PVI output currents ( $I_A, I_B, I_C$ ), load currents ( $I_{LA}, I_{LB}, I_{LC}$ ), phase-to-phase PVI output voltage before filtering ( $U_{A'B'}$ ), harmonics and imbalance correction PVI reference currents ( $I_{HI,A}^*, I_{HI,B}^*, I_{HI,C}^*$ ), as well as PV voltage ( $U_{PV}$ ), DC-link voltage ( $U_{PN}$ ), and reference DC-link voltage ( $U_{PN}^*$ ).

The CIN load current is imbalanced ( $I^-/I^+ = 10\%$ ,  $I^0/I^+ = 10\%$ ) and distorted (see Table 3) in example C (Figure 8). The grid current is out of balance and distorted because in this situation the HI compensating mechanism is not engaged. Table 4 lists the load, grid, and PVI phase currents' harmonic and imbalance components.

**Image 7.** Simulation outcomes. Case B. The values are  $P^* = 45kW$  and  $Q_1^* = 21.7KVAR$ , respectively. The CIN load is  $I_L = 30A$ . from top to bottom and left to right, as shown in Figure 6.



**Figure8:** Simulation outcomes. Case C. CIN load with harmonic components defined in Table 4 with  $P^*=45\text{ kW}$  and  $Q_1^*=15\text{ KVAR}$ . from top to bottom and left to right, as shown in Figure 6.

In Case D (Figure 9), the HIF function is engaged even though the CIN load current is distorted and imbalanced just like in Case C. It is possible to obtain balanced sinusoidal grid currents since the CIN-EMS setpoints and compensation requirements are consistent with the PVI nominal current and the converter is able to complete its assigned tasks. Table 5 lists the load, grid, and PVI phase currents' harmonic and imbalance components. THD in load currents, as can be observed, ranges from 21-28%; in contrast, THD in grid currents is noticeably lower at around 5%. Unbalances are concerned. The load currents  $I_1$  and  $I_0$  are each decreased to 0.14 and 0.2 A in the grid currents, respectively, from their original values of  $I_1=3\text{ A}$  and  $I_0=3\text{ A}$ .

**Table 4.** Harmonic and imbalance components of load, grid and PVI currents for case C.

Current	Harmonics					Imbalance			
	$I_1$ (A)	$I_3$ (A)	$I_5$ (A)	$I_7$ (A)	$I_9$ (A)	$I$ (A)	THD (%)	$I^-$ (A)	$I^0$ (A)
$i_{thc-}$	36	6.48	3.21	2.16	1.14	36.80	21.20		
$i_{Lb}$	27	6.48	3.21	2.16	1.14	28.06	28.27	3	3
$i_{Lc}$	27	6.48	3.21	2.16	1.14	28.06	28.27		
$i_{ga}$	37.59	7.02	3.66	2.54	1.16	38.56	22.92		
$i_{gb}$	45.19	6.88	3.62	2.56	1.14	45.97	18.79	3.26	3.19
$i_{gc}$	45.25	6.84	3.59	2.53	1.16	46.03	18.65		
$i_a$	68.59	0.54	0.45	0.38	0.02	68.61	3.04		
$i_b$	69.21	0.41	0.41	0.40	0.01	69.23	3.00	0.26	0.19
$i_c$	69.25	0.36	0.38	0.37	0.04	69.27	2.97		

$I_1 \dots I_9$ : RMS harmonic components;  $I$ : RMS total.  $I^-$ ,  $I^0$ : negative- and zero-sequence RMS fundamental component.

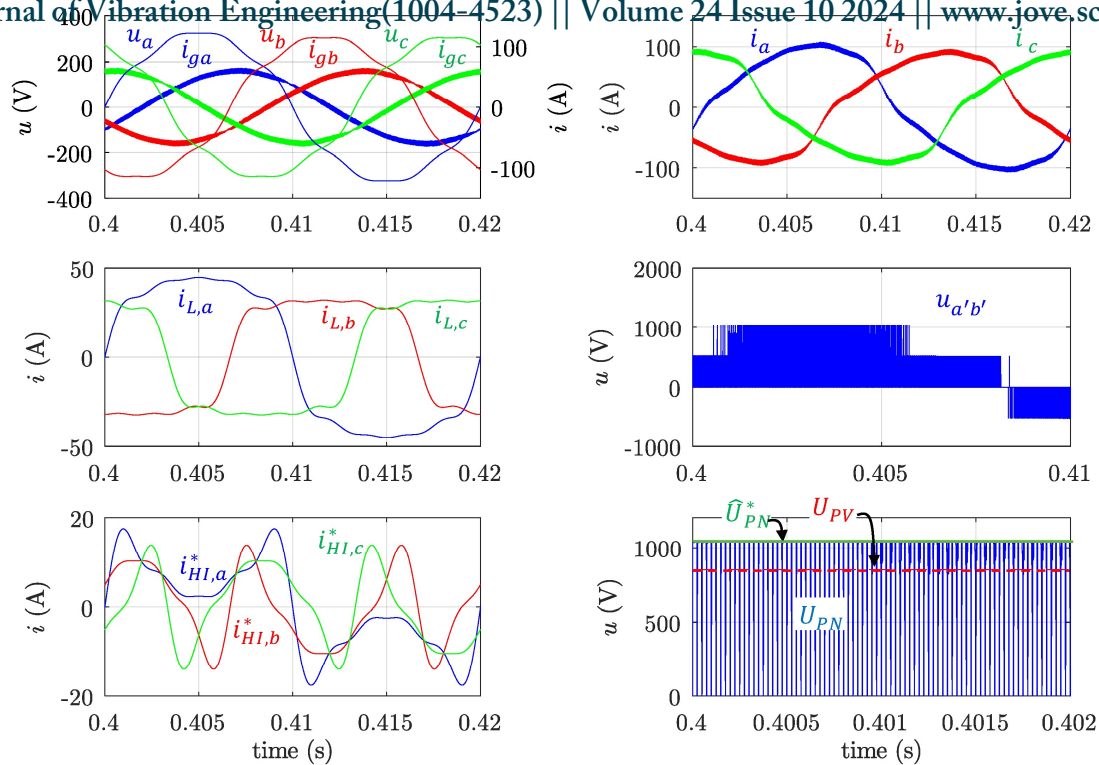


**Figure 9.** Results of the simulation. Case D. A CIN load with harmonic and unbalanced components as stated in Table 3 with  $P^* = 45 \text{ kW}$  and  $Q1^* = 15 \text{ KVAR}$ . as in Figure 6, from top to bottom and left to right.

**Table 5.** Harmonic and imbalance components of load, network and PVI currents for case D.

Current	Harmonics					Imbalance			
	$I_1 \text{ (A)}$	$I_3 \text{ (A)}$	$I_5 \text{ (A)}$	$I_7 \text{ (A)}$	$I_9 \text{ (A)}$	$I \text{ (A)}$	THD (%)	$I^- \text{ (A)}$	$I^0 \text{ (A)}$
$i_{the\_}$	36	6.48	3.21	2.16	1.14	36.80	21.20		
$i_{Lb}$	27	6.48	3.21	2.16	1.14	28.06	28.27	3	3
$i_{Lc}$	27	6.48	3.21	2.16	1.14	28.06	28.27		
$i_{ga}$	42.89	0.32	0.15	0.15	0.20	42.93	4.60		
$i_{gb}$	42.39	0.41	0.15	0.18	0.21	42.43	4.80	0.14	0.20
$i_{gc}$	42.47	0.46	0.15	0.21	0.18	42.51	4.82		
$i_a$	74.96	6.72	3.17	2.10	1.29	75.39	10.75		
$i_b$	66.04	6.88	3.20	2.05	1.31	66.54	12.43	3.13	3.20
$i_c$	66.10	6.88	3.18	2.06	1.28	66.60	12.41		

As in Cases C and D, Case E (Figure 10) exhibits the same distortion and unbalance of the CIN load current while also activating the HI function. However, the reactive power has been raised to 21.7 KVAR from the active power setpoint of 45 kW. When using these values, it is impossible to satisfy the compensation needs without overloading the machinery. Since grid currents are neither sinusoidal nor balanced, the PVI conducts a partial adjustment. The load, grid, and PVI phase currents for Case E's harmonic and imbalance components are listed in Table 6. THD at the worst phase is approximately 7.5%, and  $I^-$  and  $I^0$  are 1.81 and 1.91 A, respectively, according to grid currents, which may be observed.

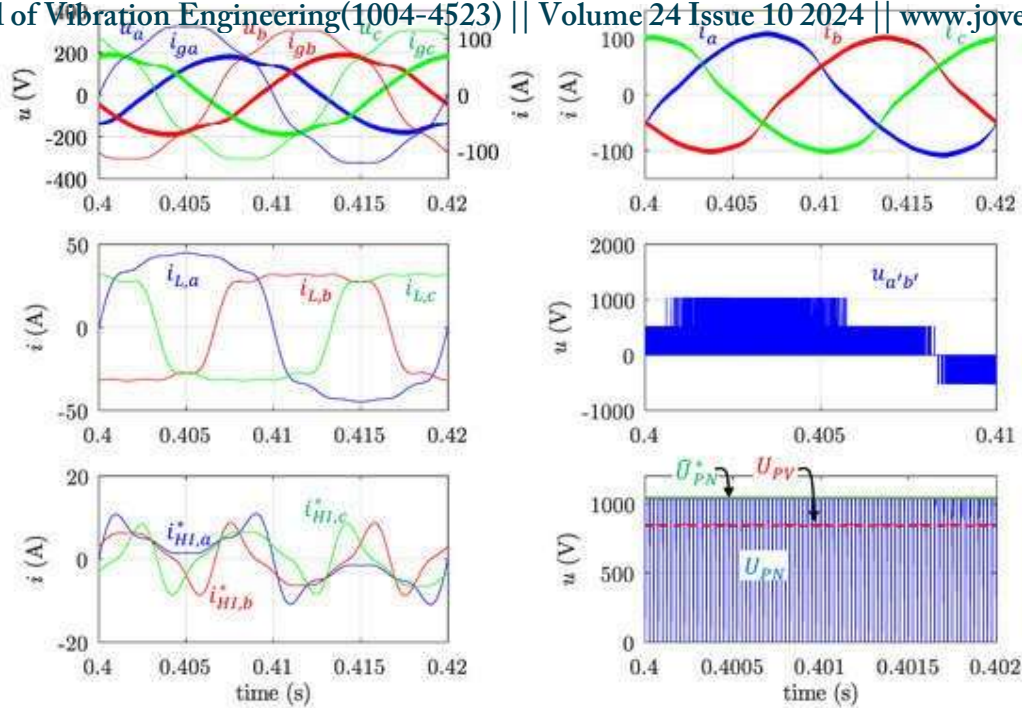


**Figure10.**Resultsofthesimulation.CaseEisaCINloadwiththesameharmonicandunbalancedcomponentsasCaseD,but with values of  $P^*=45$  kW and  $Q_1^*=21.7$  KVAR. as in Figure 6, from top to bottom and left to right.

**Table 6.** Harmonic and imbalance components of load, network and PVI currents for case E.

Current	Harmonics						Imbalance		
	$I_1$ (A)	$I_3$ (A)	$I_5$ (A)	$I_7$ (A)	$I_9$ (A)	$I$ (A)	THD (%)	$I^-$ (A)	$I^0$ (A)
$i_{the\_}$	36	6.48	3.21	2.16	1.14	36.80	21.20		
$i_{Lb}$	27	6.48	3.21	2.16	1.14	28.06	28.27	3	3
$i_{Lc}$	27	6.48	3.21	2.16	1.14	28.06	28.27		
$i_{ga}$	48.32	2.51	1.41	0.98	0.41	48.45	7.49		
$i_{gb}$	50.50	2.35	1.34	1.03	0.36	50.62	6.95	1.19	1.09
$i_{gc}$	50.56	2.37	1.42	1.09	0.39	50.68	7.07		
$i_a$	76.91	3.97	1.80	1.18	0.75	77.06	6.46		
$i_b$	71.97	4.13	1.89	1.14	0.79	72.15	7.13	1.81	1.91
$i_c$	71.98	4.12	1.79	1.08	0.76	72.15	7.05		

Numerous PVI three-phase power numbers have been determined based on the definitions suggested in Standard IEEE-1459:2010 [41]. Results for instances A through E are summarised in Table 7. The power terms listed below are displayed: real power Sink VA, real power Pink W, and real power basic reactive the displacement power factor DPF, power factor PF, power  $Q_1$  in KVAR, and inactive power N in kVA.

**Table 7.** Power terms according to IEEE-1459:2010.

CASES	S(KVA)	P(KW)	Q1(KVAR)	N(KVA)	PF	DPF
A	50.48	50.09	0.757	6.28	0.99	0.99
B	51.03	44.13	25.07	25.62	0.86	0.87
C	47.86	44.22	17.55	18.30	0.92	0.93
D	49.13	44.73	17.54	20.25	0.91	0.93
E	51.45	44.40	25.08	26.00	0.86	0.87

Figure 11 illustrates the behaviour under several setpoint settings. The total performance is detailed below:

PVI is turned on at  $t=0.2$  s and begins to inject 30 kW from the PV panels under a particular irradiation condition. The Q function is turned on at the same time to inject fundamental reactive power in the range of one-third of the active power, or 10 kVAR in this instance. Although the grid voltage is unbalanced and distorted, the PVI output current waveforms are balanced,



When the PV voltage reaches 850 V at time  $t = 0.24$  s, the DC-link voltage is controlled to its reference level ( $U_{PN}^* = 1050$  V), changing the ST ratio  $D_0$ . In both the ST and NSTU<sup>PN</sup> states, voltage  $U_{PN}$  is zero. It has been updated to reflect these changes.

The activation of the HI function causes the PVI currents to become distorted and unbalanced at  $t = 0.26$  s, while the grid currents remain sinusoidal and balanced. Due to the fact that the PVI rated power is not attained in this instance, entire compensation is feasible.

The active and reactive power setpoints are raised to  $P^* = 45$  kW and  $Q_1^* = 21.795$  KVAR, respectively, at  $t = 0.32$  s. The technology only conducts a partial correction in this situation, which leaves the grid currents slightly distorted and out of balance.

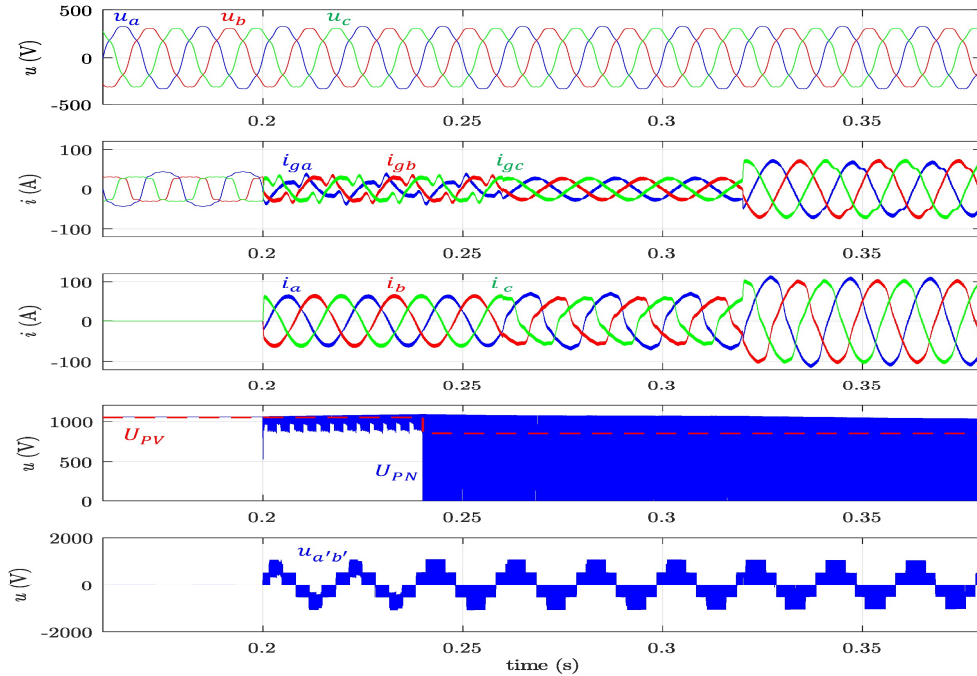


**Figure 11.** Behavior under changing setpoint conditions. From top to bottom: grid voltages ( $U_A, U_B, U_C$ ); grid currents ( $I_{GA}, I_{GB}, I_{GC}$ ); PVI output currents ( $I_A, I_B, I_C$ ); PV voltage ( $U_{PV}$ ), DC-link voltage ( $U_{PN}$ ); and phase-to-phase PVI output voltage before filtering ( $U_{A'B'}$ ).

The actual electrical models that served as the foundation for the implemented model included accurate power stage specifications. Fuji's 12MBI100VN-120-50 IGBT T-type module's datasheet was used to get a few IGBTs' key specifications. Using Tustin's technique, the transfer functions and the controllers have both been constructed in their discrete form, and all measurements are sampled before processing at a rate of 10 kHz. This sheds light on how practically feasible the plan is when made with today's quick microcontrollers.

#### IV. CONCLUSION

A control strategy has been presented for photovoltaic converters that allows the control of the overall active and reactive power of the CIN where they are integrated. Additionally, if the converter has spare capacity, the control strategy contributes to reduce the harmonic content and imbalances in the three-phase currents demanded by the entire CIN at the point of connection to the distribution network.

An interactive grid inverter is a three-phase Quasi-Z-Source Three-Level T-Type. This architecture has the potential to boost voltage and does away with the need for an extra DC-DC converter and/or a step-up transformer, both of which are frequently seen in PV inverter systems. This topology's applicability is therefore more effective for medium frequency operation than the other traditional two-level and three-level inverter architectures.

Based on the set points obtained from the CIN-EMS, it has been shown through simulation results that the reference currents can be computed locally in a time frame appropriate for practical operation, and that the currents supplied by the PVI accurately match these references. Even in the presence of distorted and imbalanced LV grid circumstances, proper functioning has been accomplished.

No cross-coupling interaction was seen, showing that the controls for active power, reactive power, and harmonic imbalance all operate separately from one another. This highlights another benefit of the suggested global control technique.

A laboratory scaled prototype is now being built, despite the implemented simulation's high level of accuracy, in order to empirically support the suggested control techniques on this topology.

This suggested PVI systems' actual application in CINs will advance the aims of the smart grid by enabling the distribution system operator to offer ancillary services and enhancing the LV network's power quality.

#### V. REFERENCES



- Journal of Vibration Engineering (1004-4525) || Volume 24 Issue 10 2024 || www.jove.science
1. Teodorescu, R.; Liserre, M.; Rodríguez, P. *Grid Converters for Photovoltaic and Wind Power Systems*; Wiley: Chichester, UK, 2010; ISBN 9780470057513.
  2. Liu, Y.; Abu-Rub, H.; Ge, B.; Blaabjerg, F.; Ellabban, O.; Loh, P.C. *Impedance Source Power Electronic Converters*; Wiley: Chichester, UK, 2016; ISBN 9781119037118.
  3. Anderson, J.; Peng, F.Z. Four Quasi-Z-Source Inverters. In *Proceedings of the 2008 IEEE Power Electronics Specialists Conference*; Rhodes, Greece, 15–19 June 2008; pp. 2743–2749.
  4. Schweizer, M.; Friedli, T.; Kolar, J.W. Comparative evaluation of advanced three-phase three-level inverter/converter topologies against two-level systems. *IEEE Trans. Ind. Electron.* 2013, 60, 5515–5527, doi:10.1109/TIE.2012.2233698.
  5. Anthon, A.; Zhang, Z.; Andersen, M.A.E.; Holmes, D.G.; McGrath, B.; Teixeira, C.A. The benefits of SiC MOSFETs in a T-type inverter for grid-tie applications. *IEEE Trans. Power Electron.* 2017, 32, 2808–2821, doi:10.1109/TPEL.2016.2582344.
  6. Husev, O.; Blaabjerg, F.; Roncero-Clemente, C.; Romero-Cadaval, E.; Vinnikov, D.; Siwakoti, Y.P.; Strzelecki, R. Comparison of impedance-source networks for two and multilevel buck–boost inverter applications. *IEEE Trans. Power Electron.* 2016, 31, 7564–7579, doi:10.1109/TPEL.2016.2569437.
  7. Ferñao Pires, V.; Cordeiro, A.; Foito, D.; Martins, J.F. Quasi-z-source inverter with a type converter in normal and failure mode. *IEEE Trans. Power Electron.* 2016, 31, 7462–7470, doi:10.1109/TPEL.2016.2514979.
  8. IEEE Recommended practice and requirements for harmonic control in electric power systems. *IEEE Std 519–2014* (Revision of IEEE Std 519–1992); IEEE: Piscataway, NJ, USA, 2014; pp. 1–29, doi:10.1109/IEEESTD.2014.6826459.